The International Journal of Cardiovascular Imaging (2019) 35:1535–1548
https://doi.org/10.1007/s10554-019-01643-4

ORIGINAL PAPER

Cross-sectional imaging of congenital pulmonary artery anomalies

Evan J. Zucker[1]

Received: 6 May 2019 / Accepted: 31 May 2019 / Published online: 7 June 2019

Abstract
Congenital pulmonary artery (PA) anomalies comprise a rare and heterogeneous spectrum of disease, ranging from abnormal origins to complete atresia. They may present in early infancy or more insidiously in adulthood, often in association with congenital heart disease such as tetralogy of Fallot or other syndromes. In recent years, cross-sectional imaging, including computed tomography (CT) and magnetic resonance imaging (MRI), has become widely utilized for the noninvasive assessment of congenital PA diseases, supplementing echocardiography and at times supplanting invasive angiography. In this article, modern CT and MRI techniques for imaging congenital PA disorders are summarized. The key clinical features, cross-sectional imaging findings, and treatment options for the most commonly encountered entities are then reviewed. Emphasis is placed on the ever-growing role of cross-sectional imaging options in facilitating early and accurate diagnosis and tailored treatment.

Keywords Pulmonary artery · Congenital · Computed tomography · Magnetic resonance imaging · Cross-sectional · Congenital heart disease

Introduction

Congenital pulmonary artery (PA) anomalies refer to a heterogeneous spectrum of disease caused by abnormal PA development [1]. Most are associated with underlying congenital heart disease (CHD) such as tetralogy of Fallot (TOF) or syndromes such as Williams and Alagille [1–3]. Broadly, congenital PA anomalies may be classified into primary disorders of PA stenosis or dilation, conotruncal abnormalities (a type of CHD), and abnormal PA origins, course, or connections [2, 4]. Clinical presentations are variable depending on the type and severity of the underlying lesion. While many PA anomalies are discovered in infancy or early childhood, others evade detection even into adulthood [1, 3].

A variety of modalities exist for imaging PA anomalies. Transthoracic echocardiography (TTE), widely available and essentially risk-free, remains the first-line test but generally underperforms for complex PA lesions [1, 5–10]. Radionuclide lung perfusion scintigraphy may be useful for assessing alterations in pulmonary blood flow related to PA abnormalities but is insufficient in isolation for characterizing PA anomalies [5, 9, 10]. Catheter angiography remains the gold standard, facilitating excellent anatomic PA delineation in addition to measurement of physiologic data such as pressure gradients and oxygen saturations. However, due to its invasive nature, it is preferably reserved for cases in which simultaneous intervention is planned [5, 8–10].

In recent years, cross-sectional imaging, including computed tomography (CT) and magnetic resonance imaging (MRI), has become widely utilized for the noninvasive assessment of congenital PA diseases, supplementing TTE and at times obviating the need for invasive angiography. In this review, cross-sectional CT and MRI techniques for imaging congenital PA anomalies are first summarized, with attention to recent advances and emerging technologies. Then, the broad spectrum of congenital PA anomalies is detailed. The central and evolving role of cross-sectional imaging in characterizing these complex disorders is emphasized, while key clinical features and treatment strategies are highlighted.

✉ Evan J. Zucker
zucker@post.harvard.edu

[1] Department of Radiology, Stanford University School of Medicine, 725 Welch Road, Stanford, CA 94305, USA

Cross-sectional imaging evaluation

Computed tomography (CT)

Multidetector CT (MDCT) with angiographic technique (CTA) has become an invaluable tool in the assessment of congenital PA disorders, facilitating rapid and precise delineation even of peripheral PA branches [5, 9–11]. Moreover, the lungs and airways and any concomitant CHD can be simultaneously evaluated [5, 6, 9, 10]. Now-ubiquitous postprocessing software facilitates the reliable and fast generation of multiplanar reformats (MPRs), maximum and minimum intensity projection reconstructions (MIPs and MinIPs, respectively), and three-dimensional (3D) reconstructions, allowing ready visualization of often complex PA anomalies both for diagnosis and pretreatment planning purposes [5, 8].

For a typical adult patient, the CTA protocol for assessing a known or suspected PA anomaly resembles what might be prescribed for assessment of pulmonary embolism. The scan range extends from the lung apices through the diaphragms, and representative scan parameters include a tube potential of 100–120 kV, tube current of 100–200 mA, detector width of 0.6 mm, and pitch of 1 (or higher if high-pitch helical mode is available) [4]. A non-ionic contrast agent, either low-osmolar (e.g., iohexol, iopamidol) or iso-osmolar (e.g., iodixanol), is administered through an 18–20 gauge (G), power-injectable, intravenous (IV) line or central catheter at a typical rate of 4–5 mL/s for a total dose of 60–150 mL, followed by a saline flush [1, 4, 5, 12]. The bolus tracking method is commonly utilized, in which a region of interest (ROI) is placed over the main PA after obtaining a single axial CT slice encompassing this anatomy. As contrast is injected, the same slice location is repeatedly imaged at regular intervals (e.g., 1 s) until a threshold Housfield unit (HU) attenuation in the ROI is achieved (e.g., 100 HU); the scan is then automatically triggered after a preset delay [12]. Alternatives to bolus tracking include the fixed scan delay method, which is less robust to individual physiology but may be simpler to implement, and the bolus timing technique, in which a small "test" bolus (e.g. 10–20 mL contrast) is used prior to the diagnostic acquisition to determine the optimal scan delay but tends to increase the total contrast dose utilized [12, 13].

In the setting of coexisting CHD or prior surgery, scan protocols may require individualization to optimize PA enhancement [1]. Achieving diagnostic acquisitions can be particularly challenging in neonates and young children, considering typical contrast dose limits of 2 mL/kg, usually requiring contrast dilution with saline to maintain a 15–25 s bolus duration while not exceeding total fluid limits of 10 mL/kg [1, 5, 6]. The IV caliber (e.g., 22–24G) is dependent on patient and may be preferentially placed in a lower rather than upper extremity vein to avoid artifact from dense contrast in the superior vena cava [5, 6]. At the same time, precautions should be taken to minimize radiation exposure (e.g., by lowering the kV to 70–80) as well as the need for sedation (e.g., by using rapid, high-pitch acquisitions if available) despite the potential for motion in "awake" patients [5, 6, 14].

Recent developments in CT have further enhanced the utility and applicability of this already robust modality for characterizing PA anomalies. Dual-source, high-pitch or volume-based acquisitions permit ever-faster scan speeds and lower radiation and contrast doses and potential sedation needs, the primary drawbacks of CT [5, 15]. Iterative reconstruction algorithms have assisted in decreasing radiation and contrast requirements while maintaining image quality, and novel image processing methods using machine/deep learning techniques may allow even further radiation/contrast reductions [5, 14, 15]. 3D printing from CT datasets is now possible and may enhance preprocedural planning [16]. Dual-energy CT (DECT) acquisition strategies, which permit greater material decomposition through the generation of distinct beam energy spectra using different tube voltages, have gained notable traction for evaluation of PA disorders [15, 17, 18]. For example, DECT post-processing software can be used to create color-coded lung iodine/perfused blood volume (PBV) maps that reflect parenchymal enhancement at a single time point and correlate with lung perfusion. In addition, "virtual" monochromatic or monoenergetic images (VMI) can be generated to simulate a lower kV, enhancing vessel contrast opacification, or higher kV, reducing beam-hardening artifact; virtual noncontrast (VNC) reconstructions can also be made to better assess calcifications and surgical material [17, 18].

More advanced photon-counting systems in which every X-ray photon generated from a CT acquisition is classified into a distinct energy bin are in development but not currently available for clinical use [15]. Fractional flow reserve (FFR)-CT, which uses computational flow modeling to assess the physiologic significance of coronary artery stenoses, has garnered increasing interest and might analogously be applied to PA stenoses in future years [15]. Finally, a novel four-dimensional (4D) flow CT method, capable of depicting and quantifying intracardiac blood flow from existing CT datasets, was recently described and might similarly prove useful for assessing PA anomalies, but its use is currently restricted to research [19].

Magnetic resonance imaging (MRI)

MRI/MR angiography (MRA) is attractive option for assessing PA anomalies given the lack of ionizing radiation and potential to achieve diagnostic imaging without contrast, or

at least using non-nephrotoxic contrast agents [18]. Moreover, intracardiac morphology and function can simultaneously be assessed in the frequent case of co-existing CHD [5, 18]. As is the case for CT, multiplanar reformations can be readily created using post-processing software when images are acquired with 3D technique [20].

Pulmonary MRA is most often performed using a rapid, time-resolved, heavily T1-weighted 3D spoiled gradient echo (SGRE) sequence [18, 20, 21]. Images are acquired over a 15–19 s breath-hold after IV administration of 0.1–0.2 mmol/kg of a gadolinium-based agent, which furthers shortens T1, at a typical flow rate of 2–5 mL/s in an adult, using bolus-tracking or bolus-timing as previously detailed [18, 21]. Traditional limitations of MRI/MRA include low spatial resolution and long acquisition times with resultant motion degradation or need for greater sedation compared to CT in young children. However, these downsides have been increasingly overcome with modern multichannel phase array coils, parallel imaging, and view-sharing technique in which central k-space is most heavily sampled [18, 21].

Noncontrast MRA is also possible, most commonly performed with a 3D steady state free precession (SSFP)/"bright blood" sequence utilizing navigator gating to ensure a constant phase of respiration and electrocardiographic (ECG) gating to maintain a constant position in the cardiac cycle [5, 18]. Furthermore, noncontrast "black blood" imaging using a two-dimensional (2D) fast spin echo (FSE) approach or the more recently described volumetric, ECG-triggered, respiratory-navigated 3D FSE technique can be informative and diagnostic when bright blood images are suboptimal due to dephasing artifact from stenosis or regurgitation [22]. In fact, compared to most alternative MRI techniques including MRA, black blood imaging is in general less prone to susceptibility artifacts, which can be generated, for example, by metallic PA stents, and potentially render other sequences nondiagnostic. Simultaneous assessment of lung perfusion is possible both with contrast-enhanced and noncontract techniques [18]. Phase contrast (PC) acquisitions can additionally be used to interrogate PA blood flow and quantify the severity of stenosis or regurgitation [5, 18]. Ultimately, however, CT is likely to be superior to MRI for certain applications such as assessment of calcifications and in-stent restenosis.

Nevertheless, several recent developments have further enhanced the speed, quality, and reliability of pulmonary MRI/MRA, solidifying its role for assessing PA anomalies. First, the advent of blood pool contrast agents, which remain in the circulation longer than do extracellular gadolinium agents, permit a longer time window for image acquisition [18]. While the gadolinium-based blood pool agent, gadofosveset, is no longer available for purchase in the United States (U.S.), there has been increasing interest in the use of ferumoxytol, an ultrasmall superparamagnetic iron oxide (USPIO) nanoparticle as an off-label contrast agent, which can be administered even in patients with renal failure [5, 18]. While adverse reactions likely occur with greater frequency when using ferumoxytol as opposed to gadolinium-based agents, the agent does appear to have a robust safety profile when administered as a slow, dilute infusion with total doses in the range of 2–4 mg/kg [5, 23, 24].

Second, 4D flow sequences, which can interrogate the morphology, function, and flow of extra- and intracardiac structures in a single 3D, 10–15 min free-breathing acquisition, and associated post-processing software, are increasingly available and now sold by several commercial vendors [5, 25]. Finally, new ultrashort echo time (UTE) sequences using radial or conical k-space sampling have facilitated much-improved assessment of the lungs and airways, historically poorly assessed by MRI, while permitting simultaneous diagnostic PA assessment [26, 27]. Comparative analysis of UTE MRI versus CT for various disease states is ongoing [28].

Disorders of pulmonary artery stenosis

Primary pulmonary arterial stenosis

PA stenosis is characterized by luminal narrowing resulting in obstruction to PA flow. Most often, it occurs at the level of the pulmonary valve, related to abnormal formation of the bulbus cordis during the 5th week of gestation [2]. However, it may be supravalvular, subvalvular, or involve peripheral PA branches, caused by intimal proliferation and fibrosis, often in association with genetic syndromes such as Williams and Alagille [1, 2, 29].

Peripheral PA stenoses, which can vary from focal narrowing to long-segment hypoplasia, are well characterized by CTA (Fig. 1a, b) [1, 2]. Use of dual-energy technique can demonstrate associated PBV deficits in the regions of stenosis [30]. MRI can similarly demonstrate the stenoses in addition to depicting and quantifying associated flow disturbances (Fig. 1c, d). In Williams patients, peripheral PA stenoses generally improve with time and are best managed expectantly, as failure rates are high with angioplasty and stenting due to the underlying arteriopathy [1, 31]. Surgical reconstruction may be considered, particularly in younger patients with severe stenoses and right ventricular (RV) hypertension [1, 32]. Transcatheter interventions appear to be more favorable in Alagille patients, although data is limited [1, 33].

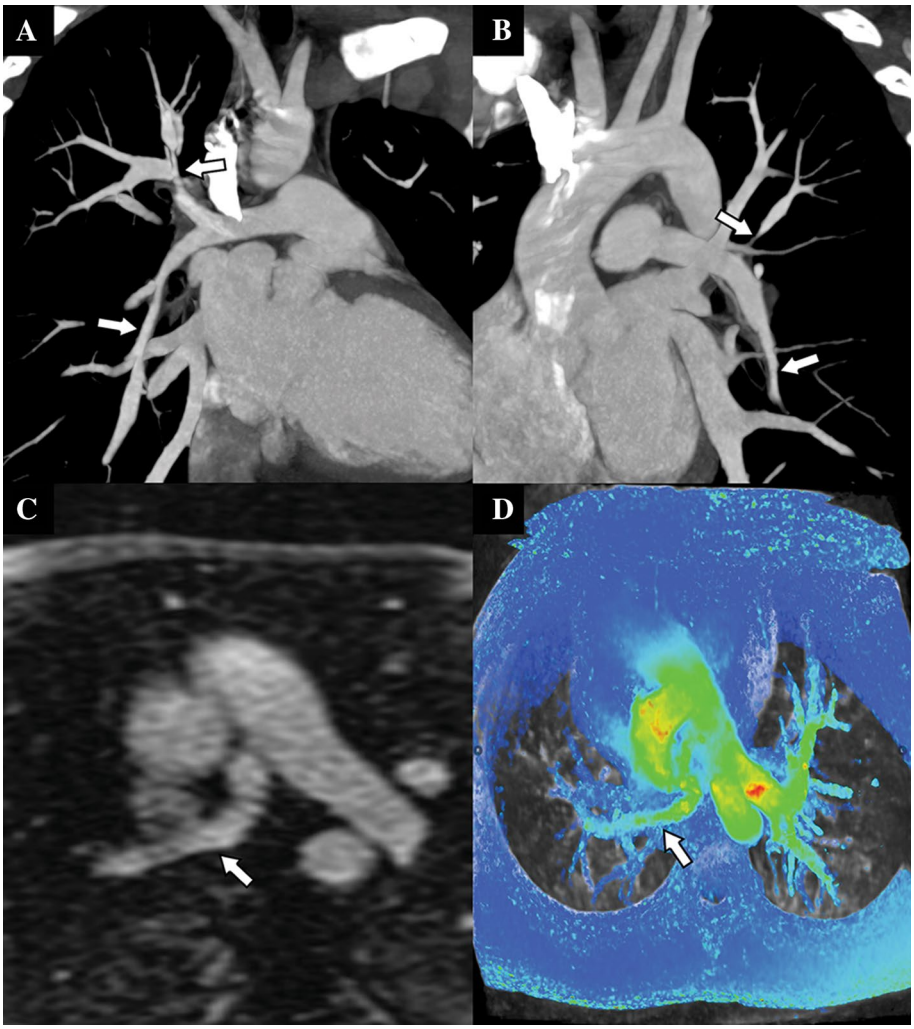

Fig. 1 *Primary pulmonary arterial stenosis*. **a**, **b** MIP reformatted chest CTA images in a 16-year-old male show multifocal, bilateral peripheral pulmonary arterial stenoses (arrows), discovered during the workup of a heart murmur. **c** Axial reformatted image from a gadobenate-enhanced, ECG-gated chest MRA performed with 3D T1-weighted SGRE technique and **d** MIP reformatted 4D flow image show a diffusely small right pulmonary artery (arrows) with kinking at the origin in a 15-year-old female with congenital right pulmonary artery hypolasia. Based on 4D flow data, there was estimated to be approximately 10% right and 90% left pulmonary arterial flow

Unilateral proximal pulmonary artery interruption

This uncommon developmental anomaly is characterized by a blind-ending either right or left PA at the hilum, potentially related to abnormal involution of one of the proximal 6th aortic arches [2, 11]. "Interruption" is the preferred term to "absence" because the intrapulmonary arteries generally remain patent and intact [11, 34]. The affected lung typically receives arterial supply from a patent ductus arteriosus (PDA) in the neonate, or in older individuals, via bronchial and transpleural collaterals [2, 11, 34, 35]. While many cases are isolated, < 1% have co-existing CHD, which is more common in left compared to right PA interruption [2, 36]. When occurring in isolation, proximal PA interruption is often asymptomatic in early childhood, but may present with exercise intolerance, recurrent pneumonia, or hemoptysis in later years [2, 36, 37].

CTA well-depicts the anomaly and associated collateralization [2]. The mediastinal portion of the PA may be nonexistent or end within 1 cm of the origin. Subpleural parenchymal lung bands may be evident, reflecting a connection between peripheral PA branches and transpleural collaterals [11]. In addition, subpleural cystic changes and bronchiectasis secondary to chronic infection or ischemia may be seen as well as potential rib notching and pleural thickening related to collateral formation [36]. DECT can demonstrate decreased PBV involving the affected lung (Fig. 2) [38]. MRI can also depict the PA interruption and be used to quantify split pulmonary lung perfusion.

For cases detected in infancy with ductal-dependent circulation, early surgical repair is recommended, as the ductus usually regresses by 1-year of age with resultant hypoplasia of the intrapulmonary arteries, decreasing the likelihood of successful surgical outcomes [2]. In later years, conservative management is preferred, although symptoms such as recurrent infection or hemoptysis may require embolization or even pneumonectomy for adequate control [2, 36]. However, by this stage, the affected lung provides little effective gas exchange, and

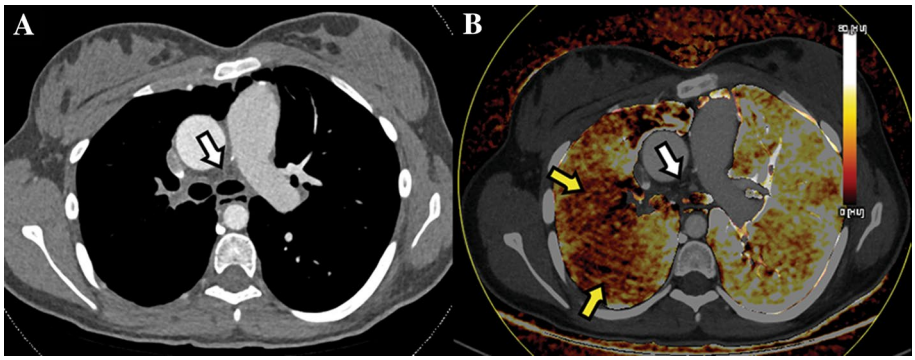

Fig. 2 *Proximal pulmonary artery interruption*. **a** Axial anatomic and **b** axial fused anatomic/PBV map images from a dual-energy chest CTA in a 13-year-old female show absence of the right PA in its expected location (white arrows), compatible with interruption. Note that lung PBV is heterogeneous but diffusely decreased on the right (yellow arrows), suggesting decreased perfusion to the right lung

thus parenchymal preservation is not of significant concern [36].

Disorders of pulmonary artery enlargement

Idiopathic pulmonary arterial hypertension

Pulmonary hypertension is defined as a mean PA pressure > 25 mmHg at rest or > 30 mmHg after exercise, as measured by right heart catheterization [11, 39]. Most cases are secondary to cardiopulmonary or hepatic disease rather than idiopathic in nature. Primary pulmonary hypertension is an idiopathic disease of the precapillary pulmonary arteries, while pulmonary veno-occlusive disease refers to an idiopathic disorder at the postcapillary, pulmonary venous level. Clinical findings are often nonspecific until progression to right heart dysfunction, associated with a poor prognosis [11].

Pulmonary artery enlargement is a characteristic feature of all forms of pulmonary hypertension (Fig. 3). In adults, a main PA diameter ≥ 29 mm is associated with an 87% sensitivity and 89% specificity for the diagnosis [11, 39]. In children, a ratio between the main PA and ascending aorta ≥ 1.2 is reported to have a sensitivity of 90% and specificity of 100% [40]. Peripheral PAs may appear abruptly attenuated, while pulmonary veins in precapillary disease appear small. Additional features may include: bronchial arterial hypertrophy, mosaic lung attenuation reflecting heterogeneous perfusion, RV dilation as evidenced by an RV to left ventricular (LV) diameter ratio > 1, and reflux of contrast in to the IVC and suprahepatic veins [11]. Lymphadenopathy in association with thickened interlobular septa and centrilobular ground-glass nodules should raise concern for pulmonary veno-occlusive disease (Fig. 3c, d) [11, 40]. The above findings are well demonstrated by CT. MRI is useful for serial assessment of RV size, function, and mass, which are prognostic markers in pulmonary hypertension (Fig. 3b) [41].

Pulmonary arterial hypertension is primarily treated with vasodilators such as inhaled nitric oxide, with 85% survival at one year. In contrast, vasodilators can precipitate life-threatening pulmonary edema in pulmonary veno-occlusive disease. In fact, bilateral lung transplantation is the only viable treatment option in this disorder, which otherwise has only a 30% survival rate at 1 year [42].

Idiopathic dilatation of the pulmonary trunk

This is a rare congenital anomaly involving, as the name implies, abnormal dilation of the main pulmonary trunk, possibly but not exclusively accompanied by right and left PA enlargement, in the absence of other identifiable causes [11]. The etiology remains uncertain; theories include unequal separation of the truncus arteriosus, congenital weakness of the PA wall, and potential underlying connective tissue disease (Fig. 4) [2]. Patients are in general asymptomatic, and the condition is usually discovered incidentally on imaging.

Both CT and MRI well-demonstrate the markedly enlarged PA; stable size across serial exams has been proposed a diagnostic criterion [11]. Signs of impending rupture may be apparent such as wall thickening reflective of subadventitial hematoma formation and perianeurysmal lung opacification. Only conservative observation is typically recommended. However, surgical repair may be considered for a main PA diameter ≥ 60 mm [2, 43].

Conotruncal malformations

Tetralogy of fallot (TOF)

TOF is the most common cause of cyanotic CHD. It is thought to be caused by malposition of the conal septum

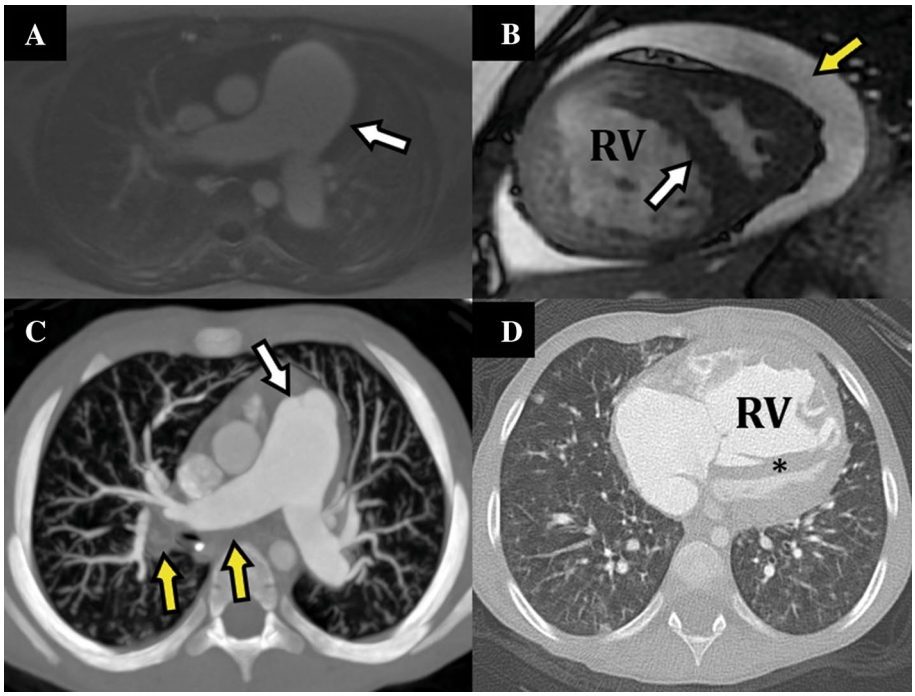

Fig. 3 *Idiopathic pulmonary arterial hypertension*. **a** Axial ferumoxytol-enhanced T1-weighted UTE image in a 20-year-old female with primary pulmonary hypertension shows an enlarged main PA (arrow). **b** Short-axis systolic SSFP image of the heart in the same patient shows an enlarged and hypertrophied right ventricle (RV) with flattening of the septum (white arrow) indicating elevated RV pressures as well as a moderate pericardial effusion (yellow arrow). **c** Axial MIP reformatted CTA image in a 3-year-old male with pulmonary veno-occlusive disease shows an enlarged main PA (white arrow) as well as tortuous, corkscrew-like peripheral PA branches. Note also the presence of subcarinal and right hilar lymphadenopathy (yellow arrows). **d** Axial CTA image in the same patient using lung windows shows a dilated and hypertrophied RV with septal flattening (asterisk) as well as bilateral, ill-defined, predominantly centrilobular ground-glass nodular opacities in the lungs

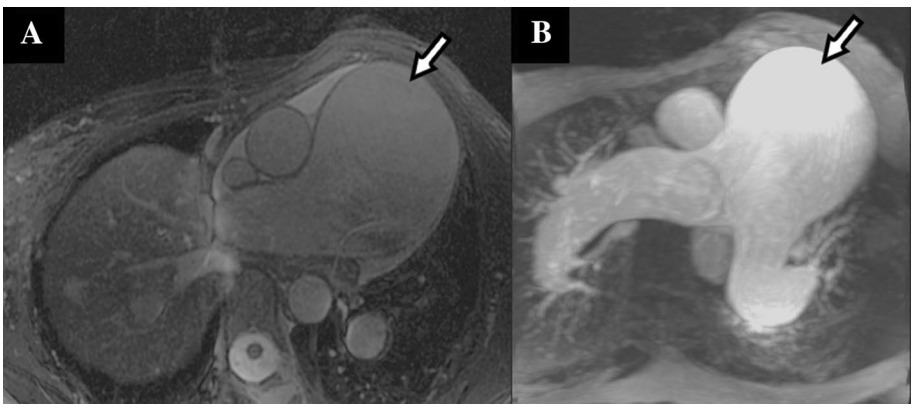

Fig. 4 *Idiopathic dilatation of the pulmonary trunk*. **a** Noncontrast axial MRA image from a respiratory-navigated, ECG-gated 3D SSFP acquisition and **b** axial MIP reformatted image from a gadobenate-enhanced, ECG-gated chest MRA performed with 3D T1-weighted SGRE technique show a markedly aneurysmal main PA (arrows), which measured > 7 cm in this 51-year-old female with Marfan syndrome

in relationship to the ventricular endocardial cushion [5, 44]. Pulmonary stenosis is a hallmark of the disorder and may be valvular, subvalvular, or supravalvular; the degree of stenosis determines the onset and severity of cyanosis. Other characteristics features of TOF are a malaligned, subaortic, membranous ventricular septal defect (VSD), an overriding aorta, and right ventricular hypertrophy (Fig. 5a, b) [5, 6, 44–47].

Several subtypes of TOF beyond the conventional form are recognized. In TOF with absent pulmonary valve, the pulmonary valve is rudimentary or nonexistent, leading to severe pulmonary regurgitation and marked enlargement of the PAs, which cause tracheobronchial compression (Fig. 5c, d). In TOF with pulmonary atresia, there is no connection between the central PAs and the right ventricular outflow tract (RVOT). This form of TOF may

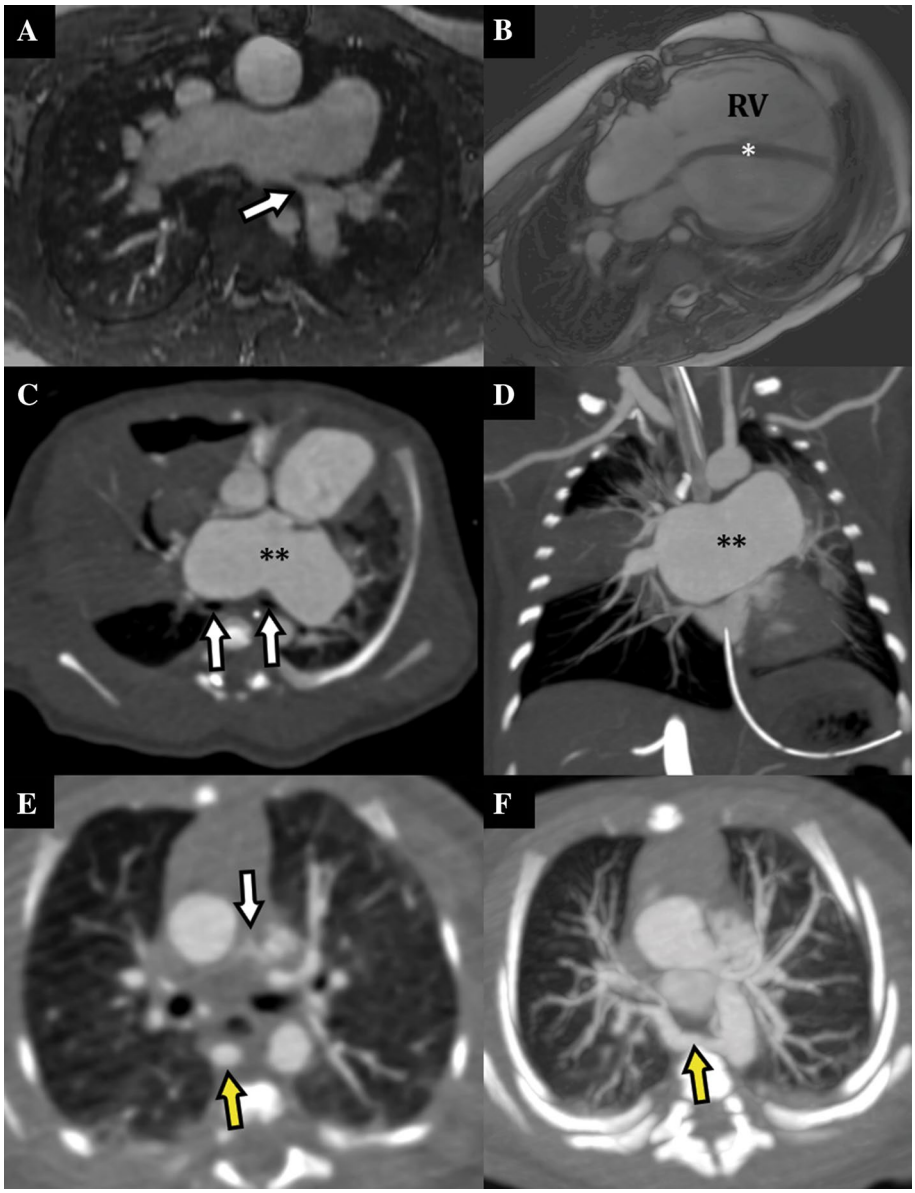

Fig. 5 *Pulmonary artery disease in tetralogy of Fallot (TOF).* **a** Axial reformatted image from a ferumoxytol-enhanced, ECG-gated chest MRA performed with 3D T1-weighted SGRE technique in a 10-year-old male with previously repaired TOF shows a severe stenosis at the left PA origin (arrow). Based on 4D flow data (not shown), there was estimated to be approximately 15% left and 85% left pulmonary arterial flow. **b** Four-chamber diastolic cine SSFP image of the heart in the same patient shows severe right ventricular (RV) enlargement with septal flattening (asterisk) compatible with RV volume overload. **c** Axial and **d** coronal MIP reformatted CTA images in a newborn with TOF and absent pulmonary valve show severe dilation of the central PAs (asterisks), which extrinsically compress the bronchi (**c**, arrows) with resultant lung atelectasis, worst in the right middle lobe. **e** Axial CTA image in a 3-day-old female with TOF, pulmonary atresia, and MAPCAs shows confluent but markedly diminutive and poorly opacified central PAs (white arrow), which had no connection to the RVOT. A large collateral in the posterior mediastinum (yellow arrow) represents a MAPCA. **f** Axial MIP reformatted image in the same patient better demonstrates the origin of the MAPCA (yellow arrow) from the descending aorta, with multiple branches supplying the right lung

be accompanied by major aortopulmonary collaterals (MAPCAs), which arise from the aorta or other arterial branches (e.g., internal mammary, intercostal, subclavian, coronary) and supply the lungs (Fig. 5e, f) [5, 12, 13, 44–47]. If present, the diminutive central PAs may be normally coalescent ("confluent") or discontinuous ("non-confluent"/"isolated").

CT provides an excellent assessment of branch PA stenoses in TOF in addition to any MAPCAs or tracheobronchial compression related to aneurysmal PAs [5, 6, 44, 48]. MRI

has a well-established role in the evaluation of postoperative TOF, performed serially to assess RV size and function and the severity of pulmonary regurgitation, helping to decide the appropriate timing for pulmonary valve replacement; the branch PAs can be concurrently assessed through MRA techniques.

The treatment of TOF depends on the severity and type of lesions involved. Definitive surgical correction is usually performed between 6 and 12 months of age, with bridging palliative procedures such as a modified Blalock–Taussig (BT) shunt if needed. Ductal-dependent TOF with pulmonary atresia is managed with prostaglandins and sometimes stenting to maintain ductal patency. MAPCAs usually require multistage operations and cardiac catheterizations to incorporate these collateral vessels into the PA circulation, a procedure known as unifocalization. Finally, TOF with absent pulmonary valve requires partial resection and repair of the aneurysmal PAs due to the potential for airway compromise [5, 6, 44–46, 48, 49].

Transposition of the great arteries (TGA)

TGA is characterized by a ventriculoarterial discordance in which the main PA arises from the left ventricle, rather than from the RV, and the aorta arises from the RV [5]. In the levo (L)—or congenitally corrected (CC)—TGA form, there is also atrioventricular discordance in which the RV arises from the left atrium and the LV arises from the right atrium; in the dextro (D)-TGA subtype, atrioventricular concordance is maintained [50, 51]. Overall, TGA is the most common cause of cyanotic CHD presenting on the first day of life. It has a male predominance and is more common in infants of diabetic mothers. Patients with D-TGA present with cyanosis by the first week of life when the ventricular septum is intact or else pulmonary edema by 2 months of age in the setting of a VSD [5]. In contrast, L-TGA may go unrecognized even into adulthood at which point the RV, functioning as the systemic ventricle, begins to fail [51].

Although echocardiography is often sufficient for initial diagnosis, both CT and MRI can accurately demonstrate the abnormal position of the main PA and aorta in the preoperative patient (Fig. 6a) [5]. These modalities are most useful in the postoperative setting for routine RV surveillance and assessment of postsurgical baffle integrity, potential stenoses at the site of reimplanted coronary arteries, and other potential complications [5, 51]. In fact, MRI has been shown to more accurately elucidate branch PA stenoses in the postoperative TGA patient compared to TTE [51, 52]. CT may be particularly helpful for assessing coronary abnormalities and when MRI is contraindicated (e.g., pacemaker, etc.) [51, 53]. In addition, either MRI (preferably) or CT can be used to serially measure LV mass if the LV needs to be "trained" by the placement of a pulmonary artery band to enable the LV to hypertrophy and function as the systemic ventricle [50].

The definitive treatment for all forms of TGA is now considered the arterial switch (Jatene) operation, in which the position of the aorta and PA are reversed, and the coronaries are reimplanted onto the neoaortic root. This is often combined with the LeCompte maneuver, in which the pulmonary root is translocated anterior to the aorta [5, 51]. However, many adult patients with TGA will have undergone an atrial switch (Mustard/Senning) procedure consisting of superior vena cava (SVC) and inferior vena cava (IVC) baffles that join and redirect systemic venous blood to the LV [51].

Truncus arteriosus

Accounting for 1% of CHD, truncus is characterized by a single semilunar (truncal) valve and single great artery that supplies the pulmonary, systemic, and coronary circulation [2, 5]. There are multiple subtypes classified according to the takeoff of the branch PAs (Fig. 6b) [5]. However, when either the right or left PA system arises entirely from the aorta and the other normally, the anatomy is termed hemitruncus (Fig. 6c) [54]. Truncus associations include DiGeorge (22q11 deletion) syndrome as well arch anomalies such as a right-sided or interrupted arch [2, 5–8]. Newborns with the disease are often initially asymptomatic but develop congestive heart failure (CHF) within several weeks as pulmonary vascular resistance drops [5].

Preoperatively, CT and MRI are not typically required. However, they may be helpful in evaluating location and branching pattern of the PAs and any MAPCAs as well as any aortic arch or pulmonary venous drainage anomalies [5]. These cross-sectional imaging modalities are routinely used postoperatively to assess biventricular and neoaortic valvular function, pulmonary regurgitation, pulmonary homograft patency, and branch PA as well as aortic anatomy and patency [5, 55, 56].

Patients with truncus usually undergo operative repair within several weeks to months of life. The surgery consists of redirecting the LV outflow toward a neoaorta in the process of VSD closure. The PAs are separated from the common arterial trunk and connected to the RV with a homograft conduit. While this RV-PA conduit may require future replacement, overall postoperative mortality rates are low [5]. Truncus has only a 5% mortality rate at one year of life if repaired, which climbs to 90% if left uncorrected [2].

Double-outlet right ventricle (DORV)

DORV refers to a ventriculoarterial discordance in which both the PA and aorta arise from the RV by at least 50% circumference (Fig. 6d) [5, 7, 46, 55, 57–60]. It is rare,

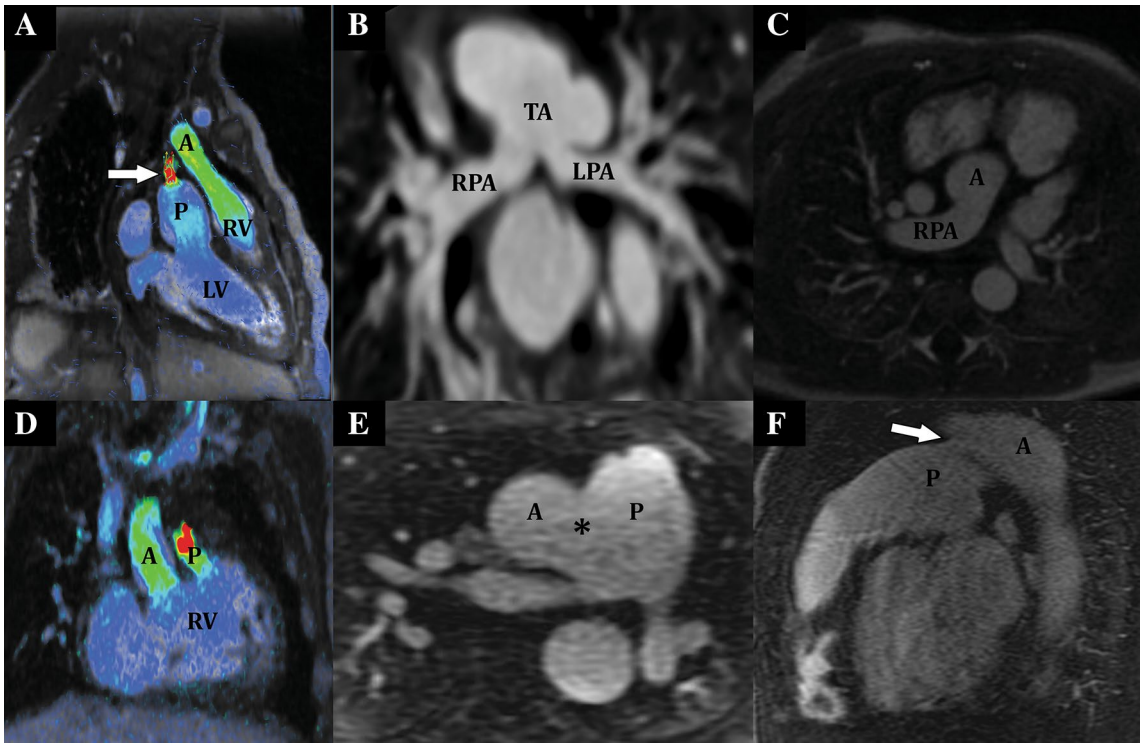

Fig. 6 *Spectrum of pulmonary artery anomalies in non-TOF conotruncal malformations*. **a** Oblique coronal image from a ferumoxytol-enhanced 4D flow acquisition in a 3-year-old male with congenitally corrected transposition of the great vessels (L-TGA) demonstrates ventriculoarterial discordance. The left ventricle (LV) is contiguous with the main pulmonary artery (P), while the right ventricle (RV) is contiguous with the aorta (A); vectors denote the direction of flow. Note the presence of flow acceleration (arrow) at the level of a PA band used to "train" the LV. **b** Curved planar reformatted image from a chest CTA performed in a 9-day-old male with truncus arteriosus type II shows a common arterial trunk (TA) with the right and left pulmonary arteries (RPA and LPA, respectively) arising in close proximity though separately from the posterior aspect of the truncus. **c** Axial image from a ferumoxytol-enhanced T1-weighted UTE acquisition in a 6-day-old male with right hemitruncus shows the right pulmonary artery (RPA) arising from the ascending aorta (A). **d** Oblique coronal image from a ferumoxytol-enhanced 4D flow acquisition in a 7-week-old female with DORV shows both the aorta (A) and main pulmonary artery (P) arising from the right ventricle (RV). **e** Axial reformatted image from a gadobenate-enhanced, ECG-gated chest MRA performed with 3D T1-weighted SGRE technique in a 16-year-old male shows a frank communication (asterisk) between ascending aorta (A) and main pulmonary artery (P) consistent with an AP window. **f** Sagittal image from the same patient and acquisition shows an additional small communication (arrow) between the pulmonary arterial trunk (P) and aortic isthmus (A), representing a patent ductus arteriosus (PDA)

accounting for < 1% of all CHD. There are 4 subtypes classified according to the location of the associated VSD and severity of associated pulmonic stenosis [5, 7, 46].

While echocardiography is generally sufficient for preoperative planning, MRI and CT can be useful in depicting the extracardiac vasculature including the PAs as well as the presence of collaterals and exact VSD morphology [5]. 3D printing has been successfully utilized in this context for depicting the complex anatomic relationships [5, 61]. In the postoperative patient with limited acoustic windows, MRI, or if contraindicated or nondiagnostic, CT is helpful for assessing the presence of PA and conduit stenoses in addition to ventricular size and function and valvular regurgitation [5, 55, 60].

DORV requires operative management, which must be tailored to the specific subtype of disease. Surgeries run the gamut from VSD closure with redirection of LV blood flow toward the aorta, to TOF or TGA-type repair, to single-ventricle type palliation Fontan creation [5, 46, 55].

Aortopulmonary (AP) window

An AP window, or aortopulmonary septal defect, is a rare anomaly characterized by an abnormal aorta-PA connection with 2 separate subarterial outflow valves and tracts. It accounts for only 0.2–0.4% of CHD [62–64]. While patients are usually symptomatic, developing progressive pulmonary arterial hypertension in the first month, asymptomatic diagnosis even in adulthood has been reported [64].

Both CT and MRI are helpful for diagnosing and characterizing the anomaly in preparation for repair (Fig. 6e). MRI

can provide the addition of flow information and quantification of shunt severity. 3D printing from cross-sectional imaging datasets may also prove beneficial [64].

Early repair in infancy is recommended to avoid long-term complications of pulmonary arterial hypertension. However outcomes after surgery appear to be favorable even with late diagnosis [63]. A variety of surgical techniques ranging from simple AP window division and suturing to transwindow access ("sandwich method") have been used with success [62]. In small, restrictive defects without other complex CHD, catheter-based closure/occlusion may be an option [63, 64].

Abnormal pulmonary artery origin, course, or connection

Pulmonary sling

Pulmonary sling refers to anomalous origin of the left PA from the right PA, attributed to maldevelopment of the 6th pulmonary arch. The aberrant LPA then courses posterior to the trachea and anterior to the esophagus [1–3]. The majority of affected patients present in the first year of life with symptoms such as stridor and dyspnea [1]. The tracheobronchial branching pattern seen with sling may be categorized according to Wells' classification: type 1A-normal; type 1B-normal except for accessory right tracheal bronchus; type 2A-low carina, distal tracheal stenosis, and bridging bronchus; and type 2B-similar to type 2A but absent or rudimentary right upper lobe bronchus [65, 66]. Type 2 branching is more common (2/3rds of cases) [1]. Approximately 30% of patients with pulmonary sling also have CHD [2].

The sling anatomy is well-assessed at CT or MRI (Fig. 7a) [1]. Concurrent tracheobronchial anomalies and compression as well as any associated CHD can be simultaneously evaluated (Fig. 7b) [2]. These factors are all important in preprocedural planning [1].

Pulmonary sling repair consists of reimplantation of the left PA onto the main PA. Any concurrent tracheal stenosis is generally repaired at the same time. The presence of long segment tracheal stenosis has been associated with mortality rates as high 22% in sling patients who otherwise have an excellent prognosis [2]. However, with advances such as slide tracheoplasty, mortality rates have declined, even reported at 0% in one series [2, 67].

Patent ductus arteriosus (PDA)

PDA is defined by a persistent communication between the main PA and descending thoracic aorta due to a lack of normal closure of the fetal ductus arteriosus. It is common, accounting for 5–10% of CHD, with a female predominance. Additional cardiac anomalies such as TGA and interrupted aortic arch may be present [6]. The PDA and associated abnormalities are well seen by cross-sectional imaging (Fig. 6f). MRI has the advantage of being able to assess the severity of associated left-to-right shunting.

In some cases, the PDA is necessary for survival, allowing oxygenated blood to mix with deoxygenated blood. In these cases, prostaglandins assist in maintaining ductal

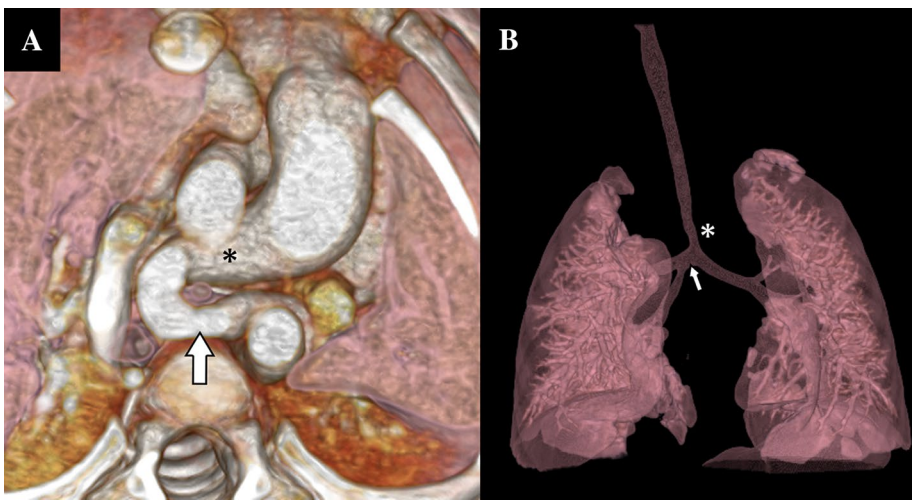

Fig. 7 *Pulmonary sling*. **a** 3D reformatted image from a chest CTA in a 13-month-old female with pulmonary sling shows the left pulmonary artery (arrow) arising abnormally from the right pulmonary artery (asterisk) and coursing posterior to the trachea. **b** 3D virtual bronchoscopic image generated from the same CTA dataset demonstrates a low carina with distal tracheal stenosis (asterisk) and a right-sided bridging bronchus (arrow) arising from the left main bronchus with absence of a true right upper lobe bronchus, findings consistent with a Wells' type 2B tracheobronchial branching pattern

patency prior to creation of a surgical shunt [1, 6]. With advances in intravascular devices, PDA stenting is now also a feasible alternative, although a technically challenging one. Pre-stent planning can be improved with the use of 3D reformats (generated from either CT or MRI acquisitions), which provide clear delineation of the shape, location, and degree of tortuosity of the ductus [1].

Abnormal coronary to pulmonary artery connections

A variety of congenital abnormal connections between the coronary and pulmonary arteries exist. In particular, coronary arteries may originate from the PAs or connect with the PAs, forming fistulae. The most common abnormal coronary origin from a PA is an anomalous left coronary from the main PA (ALCAPA) (Fig. 8a) [68]. This severe anomaly, comprising 0.25–0.5% of CHD, usually presents in infancy with symptoms related to CHF and myocardial ischemia, referred to as the Bland-White-Garland syndrome [6]. Other less common coronary origins such as an anomalous right coronary from the main PA (ARCAPA) tend to be less symptomatic [68]. If sufficient intercoronary collateral circulation develops, these anomalies may only be diagnosed incidentally in adulthood [69]. Among coronary fistulae, the main PA is the most common termination site (Fig. 8b). The overall prevalence of coronary-PA fistulae is estimated at 0.32–0.68% [70].

Both CT and MRI are well-equipped to demonstrate these anomalies and associated collateralization [69, 70]. MRI can additional be additionally used to assess for concurrent valvular or ventricular dysfunction in the setting of chronic myocardial ischemia and quantify the degree of shunting. If gadolinium is administered, inducible reversible ischemia can be identified via stress–rest perfusion MRI and infarct via late gadolinium enhancement imaging [69].

Surgical correction is recommended for ALCAPA, regardless of the timing of diagnosis and presence of irreversible myocardial scarring [69]. Coronary to pulmonary fistulae are usually treated if large, regardless of symptoms, but only if symptomatic when small-to-medium in size. For such lesions, transcatheter closure is preferred, but if unsuccessful or considered too high-risk, surgical options such as ligation vs. patch or suture closure may be pursued [69, 70].

Pulmonary arteriovenous malformation (AVM)

Pulmonary AVMs represent abnormal connections between the pulmonary and systemic circulations [71]. While their etiologies are many, including prior trauma or infection, they can arise spontaneously. The strongest association is with hereditary hemorrhagic telangiectasia (HHT), otherwise known as the Osler-Weber-Rendu syndrome, an autosomal dominant condition typified by numerous visceral AVMs [71, 72]. In fact, 80% of patients with a pulmonary AVM have HHT, and 15–45% of patients with HHT have a pulmonary AVM [72]. Clinical presentations are related to right-to-left shunting and range from dyspnea on exertion and hypoxia to cryptogenic stroke or brain abscesses to pulmonary hemorrhage [71, 72].

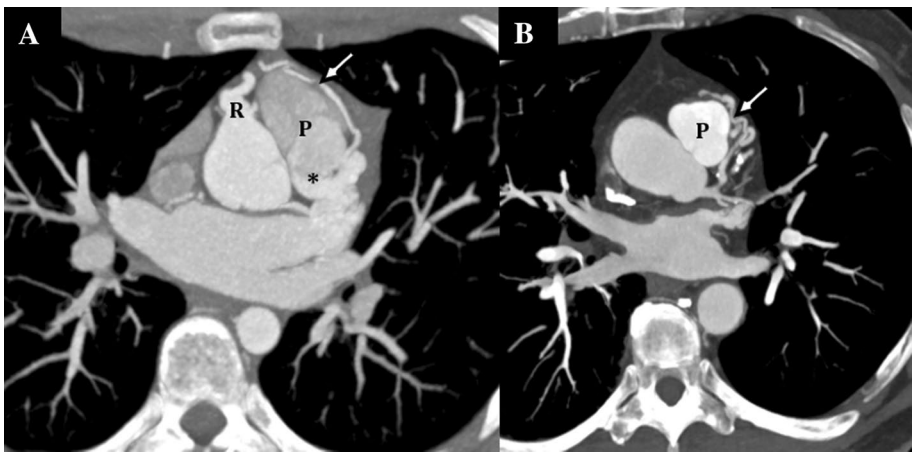

Fig. 8 *Abnormal coronary to pulmonary artery connections*. **a** Axial oblique MIP reformatted image from an ECG-gated coronary CTA in a 20-year-old male with ALCAPA shows an abnormal origin of the left main coronary artery (asterisk) from the main pulmonary artery (P). Note the compensatory large size of the right coronary artery (RCA) with right-to-left coronary collaterals (arrow). **b** Axial oblique MIP reformatted image from an ECG-gated coronary CTA in a 71-year-old male shows an abnormal tangle of vessels (arrow) arising from the left anterior descending coronary artery and converging on the main pulmonary artery (P), consistent with a coronary to pulmonary fistula

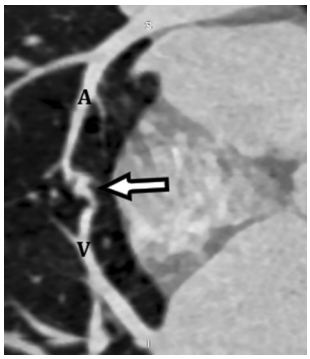

Fig. 9 *Pulmonary arteriovenous malformation (AVM).* Curved planar reformatted image from a chest CTA performed in a 5-year-old female with HHT shows an abnormal tangle of vessels (arrow) in the lung with pulmonary artery supply (A) and pulmonary venous drainage (V), consistent with an AVM

CTA is well-suited to characterizing pulmonary AVMs, which may be numerous or complex with multiple feeding arteries and draining veins (Fig. 9). The lesions tend to favor the peripheral, subpleural lower lobes [71, 72]. MIP and 3D reformats can assist in visualization [72]. In addition, DECT has been shown to demonstrate PBV deficits in the region of AVMs, potentially improving detection [73]. Embolization, rather than surgery, is now the treatment of choice for AVMs with feeding arteries ≥ 3 mm; such measurements are also accurately obtained by CT [72].

Conclusions

Cross-sectional imaging now assumes a central role in the detection and preprocedural evaluation of congenital pulmonary artery anomalies. While echocardiography in general remains the first-line test, CT and MRI are particularly well-suited to characterizing these lesions, reserving (when possible) invasive angiography for cases requiring simultaneous intervention. Recent advances in CT (e.g., dual-source and volume scanners with dual-energy capabilities) and MRI (e.g., blood pool contrast agents, 4D flow and UTE sequences) have helped to further increase the diagnostic utility of these modalities in portraying the often complex and heterogeneous anatomy involved. Continued progress in cross-sectional imaging will likely only result in more precise treatment of these often insidious yet potentially fatal disorders at the earliest opportunity.

Compliance with ethical standards

Conflict of interest No relevant relationships.

Ethical approval This article did not involve research on human participants or animals and did not require informed consent.

References

1. Dimas VV, Dillenbeck J, Josephs S (2018) Congenital pulmonary vascular anomalies. Cardiovasc Diagn Ther 8(3):214–224
2. Hirsig LE, Sharma PG, Verma N, Rajderkar DA (2018) Congenital pulmonary artery anomalies: a review and approach to classification. J Clin Imaging Sci 8:29
3. Bueno J, Flors L, Mejía M (2017) Congenital anomalies of the pulmonary arteries: spectrum of findings on computed tomography. Radiologia 59(3):209–217
4. Lin CT, Raman SP, Fishman EK (2016) An algorithmic approach to CT of pulmonary arterial disorders. Clin Imaging 40(6):1226–1236
5. Zucker EJ, Koning JL, Lee EY (2017) Cyanotic congenital heart disease: essential primer for the practicing radiologist. Radiol Clin North Am 55(4):693–716
6. Chan FP, Hanneman K (2015) Computed tomography and magnetic resonance imaging in neonates with congenital cardiovascular disease. Semin Ultrasound CT MR 36(2):146–160
7. Syamasundar Rao P (2009) Diagnosis and management of cyanotic congenital heart disease: part II. Indian J Pediatr 76(3):297–308
8. Schweigmann G, Gassner I, Maurer K (2006) Imaging the neonatal heart-essentials for the radiologist. Eur J Radiol 60(2):159–170
9. Ho VB (2008) ACR appropriateness criteria on suspected congenital heart disease in adults. J Am Coll Radiol 5(2):97–104
10. Ho VB (2009) Radiologic evaluation of suspected congenital heart disease in adults. Am Fam Physician 80(6):597–602
11. Castañer E, Gallardo X, Rimola J (2006) Congenital and acquired pulmonary artery anomalies in the adult: radiologic overview. Radiographics 26(2):349–371
12. Moore AJE, Wachsmann J, Chamarthy MR, Panjikaran L, Tanabe Y, Rajiah P (2018) Imaging of acute pulmonary embolism: an update. Cardiovasc Diagn Ther 8(3):225–243
13. Fleischmann D, Kamaya A (2009) Optimal vascular and parenchymal contrast enhancement: the current state of the art. Radiol Clin North Am 47(1):13–26
14. Kang E, Min J, Ye JC (2017) A deep convolutional neural network using directional wavelets for low-dose X-ray CT reconstruction. Med Phys 44(10):e360–e375
15. den Harder AM, Willemink MJ, de Jong PA et al (2016) New horizons in cardiac CT. Clin Radiol 71(8):758–767
16. Anwar S, Rockefeller T, Raptis DA, Woodard PK, Eghtesady P (2018) 3D printing provides a precise approach in the treatment of tetralogy of Fallot, pulmonary atresia with major aortopulmonary collateral arteries. Curr Treat Options Cardiovasc Med 20(1):5
17. Taslakian B, Latson LA, Truong MT et al (2016) CT pulmonary angiography of adult pulmonary vascular diseases: Technical considerations and interpretive pitfalls. Eur J Radiol 85(11):2049–2063
18. Tanabe Y, Landeras L, Ghandour A, Partovi S, Rajiah P (2018) State-of-the-art pulmonary arterial imaging: part 1. Vasa 47(5):345–359
19. Lantz J, Gupta V, Henriksson L et al (2018) Intracardiac flow at 4D CT: comparison with 4D flow MRI. Radiology 289(1):51–58
20. Benson DG, Schiebler ML, Repplinger MD et al (2017) Contrast-enhanced pulmonary MRA for the primary diagnosis of pulmonary embolism: current state of the art and future directions. Br J Radiol 90(1074):2016090

21. Nagle SK, Schiebler ML, Repplinger MD et al (2016) Contrast enhanced pulmonary magnetic resonance angiography for pulmonary embolism: building a successful program. Eur J Radiol 85(3):553–563
22. Henningsson M, Zahr RA, Dyer A et al (2018) Feasibility of 3D black-blood variable refocusing angle fast spin echo cardiovascular magnetic resonance for visualization of the whole heart and great vessels in congenital heart disease. J Cardiovasc Magn Reson 20(1):76
23. Hanneman K, Kino A, Cheng JY, Alley MT, Vasanawala SS (2016) Assessment of the precision and reproducibility of ventricular volume, function, and mass measurements with ferumoxytol-enhanced 4D flow MRI. J Magn Reson Imaging 44(2):383–392
24. Vasanawala SS, Nguyen KL, Hope MD et al (2016) Safety and technique of ferumoxytol administration for MRI. Magn Reson Med 75(5):2107–2111
25. Stankovic Z, Allen BD, Garcia J, Jarvis KB, Markl M (2014) 4D flow imaging with MRI. Cardiovasc Diagn Ther 4(2):173–192
26. Zucker EJ, Cheng JY, Haldipur A, Carl M, Vasanawala SS (2018) Free-breathing pediatric chest MRI: performance of self-navigated golden-angle ordered conical ultrashort echo time acquisition. J Magn Reson Imaging 47(1):200–209
27. Higano NS, Fleck RJ, Spielberg DR et al (2017) Quantification of neonatal lung parenchymal density via ultrashort echo time MRI with comparison to CT. J Magn Reson Imaging 46(4):992–1000
28. Burris NS, Johnson KM, Larson PE et al (2016) Detection of small pulmonary nodules with ultrashort echo time sequences in oncology patients by using a PET/MR system. Radiology 278(1):239–246
29. van Son JA, Edwards WD, Danielson GK (1994) Pathology of coronary arteries, myocardium, and great arteries in supravalvular aortic stenosis. Report of five cases with implications for surgical treatment. J Thorac Cardiovasc Surg 108(1):21–28
30. Zucker EJ, Kino A, Schmiedeskamp H, Hinostroza V, Fleischmann D, Chan FP (2019) Feasibility and utility of dual-energy chest CTA for preoperative planning in pediatric pulmonary artery reconstruction. Int J Cardiovasc Imaging. https://doi.org/10.1007/s10554-019-01602-z
31. Collins RT 2nd (2013) Cardiovascular disease in Williams syndrome. Circulation 127(21):2125–2134
32. Mainwaring RD, Hanley FL (2017) Surgical techniques for repair of peripheral pulmonary artery stenosis. Semin Thorac Cardiovasc Surg 29(2):198–205
33. Zussman M, Hirsch R, Beekman RH 3rd, Goldstein BH (2015) Impact of percutaneous interventions for pulmonary artery stenosis in Alagille syndrome. Congenit Heart Dis 10(4):310–316
34. Kieffer SA, Amplatz K, Anderson RC, Lillehei CW (1965) Proximal interruption of a pulmonary artery. Am J Roentgenol Radium Ther Nucl Med 95(3):592–597
35. Sherrick DW, Kincaid OW, Dushane JW (1962) Agenesis of a main branch of the pulmonary artery. Am J Roentgenol Radium Ther Nucl Med 87:917–928
36. Williams EA, Cox C, Chung JH, Grage RA, Rojas CA (2019) Proximal interruption of the pulmonary artery. J Thorac Imaging 34(1):56–64
37. Apostolopoulou SC, Kelekis NL, Brountzos EN, Rammos S, Kelekis DA (2002) "Absent" pulmonary artery in one adult and five pediatric patients: imaging, embryology, and therapeutic implications. AJR Am J Roentgenol 179(5):1253–1260
38. Yoshida R (2019) Clinical case dual energy: absence of a pulmonary artery. https://health.siemens.com/ct/image-contest/show/index/303/absence-of-a-pulmonary-artery/1. Accessed 5 May 5 2019
39. Frazier AA, Galvin JR, Franks TJ, Rosado-De-Christenson ML (2000) From the archives of the AFIP: pulmonary vasculature: hypertension and infarction. Radiographics 20(2):491–524
40. Berteloot L, Proisy M, Jais JP et al (2019) Idiopathic, heritable and veno-occlusive pulmonary arterial hypertension in childhood: computed tomography angiography features in the initial assessment of the disease. Pediatr Radiol 49(5):575–585
41. Bourji KI, Hassoun PM (2015) Right ventricle dysfunction in pulmonary hypertension: mechanisms and modes of detection. Curr Opin Pulm Med 21(5):446–453
42. Balko R, Edriss H, Nugent K, Test V (2017) Pulmonary veno-occlusive disease: an important consideration in patients with pulmonary hypertension. Respir Med 132:203–209
43. Kharge J, Singh AP, Raghu TR, Hegde M, Bharata A, Manjunath CN (2013) Idiopathic dilatation of the pulmonary artery: a case report. Echocardiography 30(9):E265–E268
44. Gartner RD, Sutton NJ, Weinstein S, Spindola-Franco H, Haramati LB (2010) MRI and computed tomography of cardiac and pulmonary complications of tetralogy of fallot in adults. J Thorac Imaging 25(2):183–190
45. Rao PS (2009) Diagnosis and management of cyanotic congenital heart disease: part I. Indian J Pediatr 76(1):57–70
46. Rao PS (2013) Consensus on timing of intervention for common congenital heart diseases: part II. cyanotic heart defects. Indian J Pediatr 80(8):663–674
47. Puranik R, Muthurangu V, Celermajer DS, Taylor AM (2010) Congenital heart disease and multi-modality imaging. Heart Lung Circ 19(3):133–144
48. Malhotra SP, Hanley FL (2009) Surgical management of pulmonary atresia with ventricular septal defect and major aortopulmonary collaterals: a protocol-based approach. Semin Thorac Cardiovasc Surg Pediatr Card Surg Annu 12(1):145–151
49. Gaca AM, Jaggers JJ, Dudley LT, Bisset GS 3rd (2008) Repair of congenital heart disease: a primer: part 2. Radiology 248(1):44–60
50. Mainwaring RD, Patrick WL, Ibrahimiye AN, Watanabe N, Lui GK, Hanley FL (2018) An analysis of left ventricular retraining in patients with dextro- and levo-transposition of the great arteries. Ann Thorac Surg 105(3):823–829
51. Gaydos SS, Varga-Szemes A, Judd RN, Suranyi P, Gregg D (2017) Imaging in adult congenital heart disease. J Thorac Imaging 32(4):205–216
52. Weiss F, Habermann CR, Lilje C et al (2005) MRI of pulmonary arteries in follow-up after arterial-switch-operation (ASO) for transposition of great arteries (D-TGA). Rofo 177(6):849–855
53. Cohen MS, Eidem BW, Cetta F et al (2016) Multimodality imaging guidelines of patients with transposition of the great arteries: a report from the American Society of Echocardiography developed in collaboration with the Society for Cardiovascular Magnetic Resonance and the Society of Cardiovascular Computed Tomography. J Am Soc Echocardiogr 29(7):571–621
54. Haywood LJ, Chakryan Y, Kim D, Boltzer T, Rivas G, Shavelle D (2014) Abnormal origin of the right pulmonary artery from ascending aorta (hemitruncus arteriosus). J Investig Med High Impact Case Rep 2(3):2324709614536139
55. Frank L, Dillman JR, Parish V et al (2010) Cardiovascular MR imaging of conotruncal anomalies. Radiographics 30(4):1069–1094
56. Agrawal R, Ghoshhajra B, Kovacina B et al (2012) Truncus arteriosus. MGH Cardiovascular Images eNewsletter 2012(45). https://www.massgeneral.org/imaging/news/cv-newsletter/march_2012/. Accessed 5 May 2019
57. Shi K, Yang ZG, Chen J, Zhang G, Xu HY, Guo YK (2015) Assessment of double outlet right ventricle associated with multiple malformations in pediatric patients using retrospective ECG-gated dual-source computed tomography. PLoS ONE 10(6):e0130987
58. Goo HW, Park IS, Ko JK (2003) CT of congenital heart disease: normal anatomy and typical pathologic conditions. Radiographics 23:147–165

59. Chen SJ, Lin MT, Liu KL et al (2008) Usefulness of 3D reconstructed computed tomography imaging for double outlet right ventricle. J Formos Med Assoc 107(5):371–380
60. Saremi F, Ho SY, Cabrera JA et al (2013) Right ventricular outflow tract imaging with CT and MRI: part 1, morphology. AJR Am J Roentgenol 200(1):W39–W50
61. Bharati A, Garekar S, Agarwal V et al (2016) MRA-based 3D-printed heart model-an effective tool in the pre-surgical planning of DORV. BJR Case Rep 2:20150436
62. Talwar S, Agarwal P, Choudhary SK et al (2017) Aortopulmonary window: morphology, diagnosis, and long-term results. J Card Surg 32(2):138–144
63. He J, Yan D, Li B, Li H (2018) Surgical repair of complex aortopulmonary window: a case study. Braz J Cardiovasc Surg 33(4):424–427
64. Balegadde AV, Vijan V, Thachathodiyl R, Kappanayil M (2018) A case of asymptomatic large aortopulmonary window in an adult: role of cardiac CT, CMRI, and 3D printing technology. Anatol J Cardiol 19(1):72–74
65. Zhong YM, Jaffe RB, Zhu M, Gao W, Sun AM, Wang Q (2010) CT assessment of tracheobronchial anomaly in left pulmonary artery sling. Pediatr Radiol 40(11):1755–1762
66. Wells TR, Gwinn JL, Landing BH, Stanley P (1988) Reconsideration of the anatomy of sling left pulmonary artery: the association of one form with bridging bronchus and imperforate anus. Anatomic and diagnostic aspects. J Pediatr Surg 23(10):892–898
67. Yong MS, d'Udekem Y, Brizard CP et al (2013) Surgical management of pulmonary artery sling in children. J Thorac Cardiovasc Surg 145(4):1033–1039
68. Williams IA, Gersony WM, Hellenbrand WE (2006) Anomalous right coronary artery arising from the pulmonary artery: a report of 7 cases and a review of the literature. Am Heart J 152(5):1004.e9–17
69. Agarwal PP, Dennie C, Pena E et al (2017) Anomalous coronary arteries that need intervention: review of pre- and postoperative imaging appearances. Radiographics 37(3):740–757
70. Verdini D, Vargas D, Kuo A et al (2016) Coronary-pulmonary artery fistulas: a systematic review. J Thorac Imaging 31(6):380–390
71. Dupuis-Girod S, Cottin V, Shovlin CL (2017) The lung in hereditary hemorrhagic telangiectasia. Respiration 94(4):315–330
72. Cummings KW, Bhalla S (2010) Multidetector computed tomographic pulmonary angiography: beyond acute pulmonary embolism. Radiol Clin North Am 48(1):51–65
73. Kim BH, Seo JB, Chae EJ, Lee HJ, Hwang HJ, Lim C (2012) Analysis of perfusion defects by causes other than acute pulmonary thromboembolism on contrast-enhanced dual-energy CT in consecutive 537 patients. Eur J Radiol 81(4):e647–652